

Convective heat transfer coefficient in compartment fires

Journal of Fire Sciences

31(5) 410–423

© The Author(s) 2013

Reprints and permissions:

sagepub.co.uk/journalsPermissions.nav

DOI: 10.1177/0734904113479001

jfs.sagepub.com



Peter S Veloo¹ and James G Quintiere²

Date received: 25 January 2013; accepted: 27 January 2013

Abstract

Heat transfer to compartment surfaces was measured in fully developed fire experiments. The experiments involved scaled compartments ranging from 1/8th to 3/8th with full-scale height of 2.54 m. Gas temperatures reached 1000°C, and total surface heat flux could reach 200 kW/m², with convection accounting for 25% of the total. A combination of thermopile heat flux gage, metal plate sensor, and gas and wall thermocouples was used to separate the convective and radiative components. The convective heat transfer coefficients were resolved experimentally. Convective heat transfer coefficient was correlated against temperature rise within the compartment for both flaming and after extinction phases.

Keywords

Scale modeling, compartment fire, heat transfer, radiation, convection, convective heat transfer coefficient

Introduction

Heat transfer via convection is usually downplayed in fire applications, as radiation dominates the burning rate for fires above 1 m in scale. At the early stage of the fire, convection is appreciated to be more important, especially in the activation of thermal alarms and sprinklers. Yet, in fully developed fire, the role of convection has not been actively explored. Indeed, in the consideration of the effect of fire on structures (e.g. beams and columns), the convective heat transfer coefficient is usually taken as some extrapolation of normal heat transfer. This is especially troubling when the cooling period following extinction in a fire is

¹Department of Mechanical and Aerospace Engineering, Princeton University, Princeton, NJ, USA

²Department of Fire Protection Engineering, University of Maryland, College Park, MD, USA

Corresponding author:

Peter S Veloo, Department of Mechanical and Aerospace Engineering, Princeton University, Princeton, NJ 08544, USA.

Email: pveloo@princeton.edu

modeled as an empirical factor based on a constant temperature rate. Even the popular fire dynamics simulator (FDS) code addresses convection heat transfer in an empirical manner.¹ The FDS guide shows that it cannot resolve the boundary and only approximates the heat transfer coefficient through correlations from forced convection heat transfer on a flat plate receiving uniform velocity. Furthermore, FDS assumes a length scale. Knowledge of the convective heat transfer coefficient could serve to offer a better model.

Very limited studies have been performed to resolve experimentally the heat transfer coefficient in fire applications. Veldman et al.² and Zukoski and Kubota³ used a thin plate calorimeter to measure and correlate the convective heat transfer coefficient to a ceiling due to fire plume impingement. They studied both unconfined² and confined³ ceilings and correlated their results with the dimensionless energy release rate, Q^* (or Zukoski number). The focus of the studies by Veldman et al.² and Zukoski and Kubota³ was to determine the convective heat transfer coefficient at conditions similar to those encountered in the early stages of a fire, before a room becomes completely involved in flames. You and Faeth⁴ investigated ceiling heat fluxes for both confined and unconfined ceilings. Their study was also focused on the initial stages of ceiling heating by fire conditions. They demonstrated that ceiling heat fluxes were relatively independent of position.

Cooper⁵ and Cooper and Stroup⁶ studied heat transfer to unconfined ceilings. An algorithm was developed to account for the convective heat transfer from a buoyant plume-driven ceiling jet to the ceiling surface. Beyler⁷ performed a review of expressions describing plume and ceiling jet flow from the literature. These expressions were used to predict convective heat transfer from these flows. Alpert⁸ measured convective heat flux to confined ceilings at Reynolds numbers that was an order of magnitude above previous studies by performing laboratory scale experiments at elevated ambient pressure. They demonstrated that plume buoyancy causes heat transfer rates in the impingement region of the ceiling that are different from forced convection relations.⁸

Later, Tanaka and Yamada⁹ studied methanol pool fires in nearly closed cubic compartments of 0.5 and 1.5 m to measure the overall heat transfer coefficient. They not only formed a correlation in terms of Q^* , but also noted a dependency on the temperature rise in the compartment. As temperature is the driving force for compartment flow, and convective heat transfer is velocity and scale dependent, we later explored the correlation approach that was suggested by Tanaka and Yamada.⁹ While the Tanaka and Yamada⁹ results are primarily for low temperatures, we explore the high temperature range of fully developed fires. It will additionally be demonstrated, in later sections, that present results subsume those from Tanaka and Yamada.⁹

The compartment experiments of our study spring from a bigger set of studies that explored the use of scale models in predicting the effect of fire on structures.¹⁰⁻¹⁴ The selection of the full-scale compartment dimensions, ventilation, the requirement for the full-scale burn time and fuel loading, and the compartment material for the full scale have been discussed in detail in these previous publications. Perricone et al.,¹⁰ Perricone,¹² Wang et al.,¹¹ and Wang¹³ experimentally validated the theoretical method of scale modeling and demonstrated transient and spatial accuracies of reaction rates, temperature, and gas composition in ventilation-limited enclosures at three different scales. These fires involved wood cribs and compartment scales of 1/8, 1/4, and 3/8 of a benchmark compartment with dimensions $3.76 \times 3.76 \times 2.54$ m.

Measurements were then made to validate the ability to scale the transient heat flux in compartment fires using a commercial thermopile water-cooled gage and a fabricated thin

plate gage. Further discussion of the scaling results for heat flux can be found in Veloo.¹⁴ The focus of this article is on the results for the measured convective heat transfer coefficient in compartment fires.

The use of a plate thermometer has been made before in fire applications (e.g., Wickström,^{15,16} Lennon and Silcock,^{17,18} and Zhang and Delichatsios¹⁹) but not in this fully developed compartment fire scenario to obtain the heat transfer coefficient. Wickström¹⁵ introduced a plate thermometer that was initially utilized to determine heat transfer conditions in furnaces. The sensor was a thin steel plate with insulating fiber board on one side and a thermocouple welded to the center of the plate. This plate sensor methodology was then used in conjunction with the adiabatic surface temperature methodology¹⁶ to determine both convection and radiation heat transfers in an enclosure with a gas burner. Lennon and Silcock^{17,18} developed a Thin Plate Device (TPD) to economically measure incident heat flux in both the enclosure and furnace fires. The TPD consists of a pair of thin metal disks, one with high emissivity and the other with low emissivity. Back conduction losses were ignored during calibration. Zhang and Delichatsios¹⁹ determined instantaneous convective heat transfer coefficients using a thin steel plate probe similar in design to that of Wickström^{15,16} combined with a Gardon heat flux gage (HFG). Three-dimensional (3D) numerical calculations were used to solve for the back conduction losses from the sensor.

In this article, we will first rigorously describe our plate sensor design. Following which, we will describe the methodology used to measure the heat transfer coefficient in the compartment fires. Finally, we will present some results and then present the dimensionless correlations.

Experimental methodology

The concept of the plate sensor is to establish, by calibration, its rear substrate heat loss, time response, and effective heat capacity. Then, its implementation is to treat it like a first-order linear time response device and correct its “steady” reading to the measurement. An examination of the calibration process will reveal the details of this process.

The sensor design is depicted in Figure 1, with a plate of 2-mm-thick steel painted with Medtherm® HFG paint of known emissivity of 0.9. A K-type thermocouple was spot welded on the rear of the metal plate. The temperature of the plate is then recorded over time as its front surface is exposed to a heat source and its rear is heavily insulated. A total of 10 sensors were made, and their individual calibration will be outlined next.

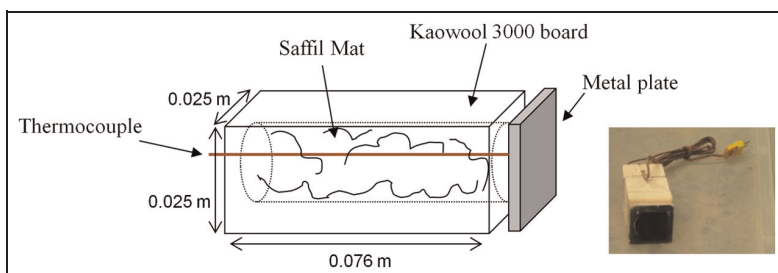


Figure 1. Metal plate sensor.

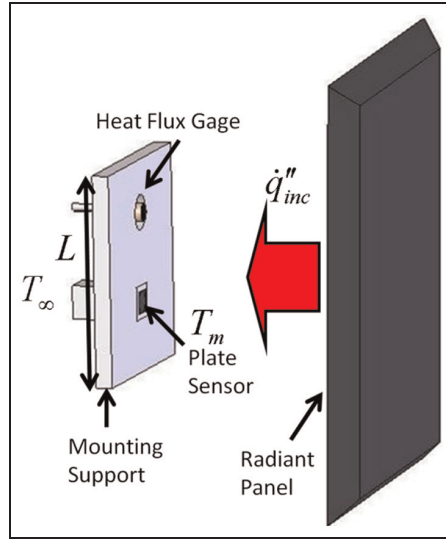


Figure 2. Calibration arrangement.

Sensor calibration

A schematic of the calibration arrangement is shown in Figure 2 in which incident radiant heat flux, \dot{q}''_{inc} , from a high-temperature gas fired panel is imposed on an inert board containing the plate sensor and a water-cooled Medtherm (Schmidt-Boelter) thermopile HFG. The Medtherm HFG has a diameter of 25.4 mm, is accurate to within $\pm 5\%$, and linear between 10 and 200 kW/m². The plate sensor response is given by equation (1)

$$\left(\frac{mc}{A}\right)_m \frac{dT_m}{dt} = \alpha_m \dot{q}''_{inc} - \sigma \epsilon_m (T_m^4 - T_\infty^4) - h_{c,plate} (T_m - T_\infty) - \dot{q}''_{cond,m} \tag{1}$$

The ambient temperature is taken to be the measured laboratory temperature at the time of calibration. The subscript “m” refers to the metal plate, and the full description of symbols is given in Appendix 1, Notation.

At steady state, equation (1) can be solved to give the conduction losses to the rear substrate. This is achieved by measuring the total incident heat flux using the water-cooled upper Medtherm gage and recording the plate temperature. The plate sensor absorptivity and emissivity are set to the value of the paint of 0.9. Finally, the convective heat transfer losses from the plate sensor can be estimated using an approximation for the convective heat transfer coefficient from the plate from natural convection correlations for a vertical plate. We have assumed that radiation is completely to the ambient surroundings. The steady-state expression for the conduction loss is then

$$\dot{q}''_{cond,m} = \alpha_m \dot{q}''_{inc} - \sigma \epsilon_m (T_m^4 - T_\infty^4) - h_{c,plate} (T_m - T_\infty) \tag{2}$$

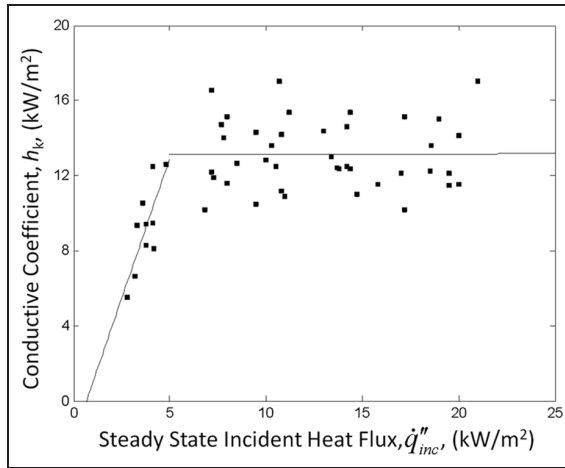


Figure 3. Conduction coefficient as a function of incident heat flux.

Because this heat loss into the insulation is expected to be relatively small, such steady estimates are reasonable even applied during the transient period. Furthermore, the conductive loss is estimated as linear in plate to ambient temperature difference, that is

$$h_k = \frac{\alpha_m \dot{q}''_{inc} - \sigma \epsilon_m (T_m^4 - T_\infty^4) - h_{c,plate} (T_m - T_\infty)}{(T_m - T_\infty)} \tag{3}$$

Figure 3 shows that the conductive heat transfer coefficient, h_k , for all 10 metal plate sensors can be taken as a function of the incident heat flux and will be used in application later in the compartment measurements. In essence, above an incident heat flux of 5 kW/m^2 , h_k is $13 \text{ W/m}^2 \text{ K}$. The scatter arises from using 10 individual sensors and construction imperfections. In this approximate fashion, a conduction heat loss is estimated in the plate measurement.

In addition to linearizing the conduction loss with temperature, plate reradiation is treated in a similar way. With this in mind, equation (1) can be rewritten as

$$\left(\frac{mc}{A}\right)_m \frac{dT_m}{dt} = \alpha_m \dot{q}''_{inc} - h_{eff} (T_m - T_\infty) \tag{4}$$

where h_{eff} represents

$$h_{eff} = h_{c,plate} + h_k + \sigma \epsilon_m (T_m^2 + T_\infty^2) (T_m + T_\infty) \tag{5}$$

Now consider the measured metal plate sensor heat flux expressed as

$$\dot{q}''_m = \sigma \epsilon (T_m^4 - T_\infty^4) + h_{c,plate} (T_m - T_\infty) + h_k (T_m - T_\infty) \equiv h_{eff} (T_m - T_\infty) \tag{6}$$

In this calibration mode, the plate reading can be derived from the instantaneous temperature measurement according to the substitution into equation (5). However, if we wish to

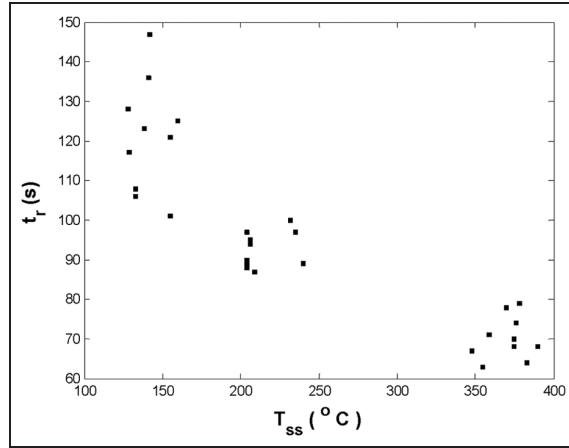


Figure 4. Metal plate sensor time response as a function of steady state plate temperature.

derive the incident radiant heat flux from this plate reading, we must revert to the following equation that follows from the definition of \dot{q}''_m in equations (4) and (6)

$$\left(\frac{mc}{A}\right)_m \frac{1}{h_{eff}} \frac{d\dot{q}''_m}{dt} + \dot{q}''_m = \alpha_m \dot{q}''_{inc} \tag{7}$$

The terms embracing the coefficient of the derivative in equation (7) are the time constant of the device, t_r , and need not be computed from its components. More empirically, the time constant can be derived from the calibration tests. Applying an incident radiant heat flux and recording the plate temperature over time allows for the computation of \dot{q}''_m and its time derivative, following which t_r can be resolved using equation (7). The time constant, t_r , is shown as a function of plate temperature in Figure 4. The time constant is a function of temperature due to its dependence on h_{eff} .

However, the remainder of the time constant term is primarily a constant, despite some temperature effects in the specific heat term. This is shown by processing the data in Figure 4 with the corresponding h_{eff} term. Figure 5 shows the constancy of mc/A , and it will be taken as a constant for the plate gage as $3.2 \text{ kJ/m}^2 \text{ K}$.

The heat capacity per unit area and the heat loss by conduction through the rear insulation are taken as two properties constant of the plate gage: mc/A is $3.2 \text{ kJ/m}^2 \text{ K}$ and h_k is $13 \text{ W/m}^2 \text{ K}$ for most applications. The gage can now be used in other applications, such as heating in a compartment in which the incident heat flux is from convection and radiation. The application of equation (7) is the operation of the gage and will give the incident heat flux (radiation plus convection in the compartment). This process will be explicitly laid out in the next section. However, to see that the process can be applied to the calibration application in which the incident radiant heat flux is constant for a run, Figure 6 shows the results of the direct measure of gage and the incident flux computed by equation (7).

There are three curves depicted in Figure 6: the incident heat flux that is measured by the thermopile gage, the measured metal plate gage heat flux, and the corrected plate gage heat flux. The corrected heat flux $\dot{q}''_{m,corr}$ is determined by computing the left-hand side of

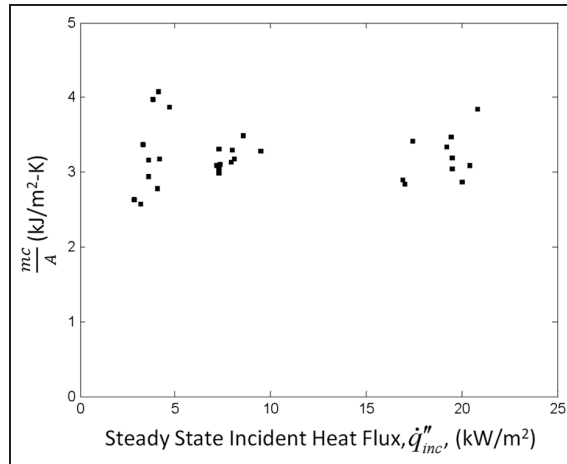


Figure 5. Heat capacity per unit area of plate gage.

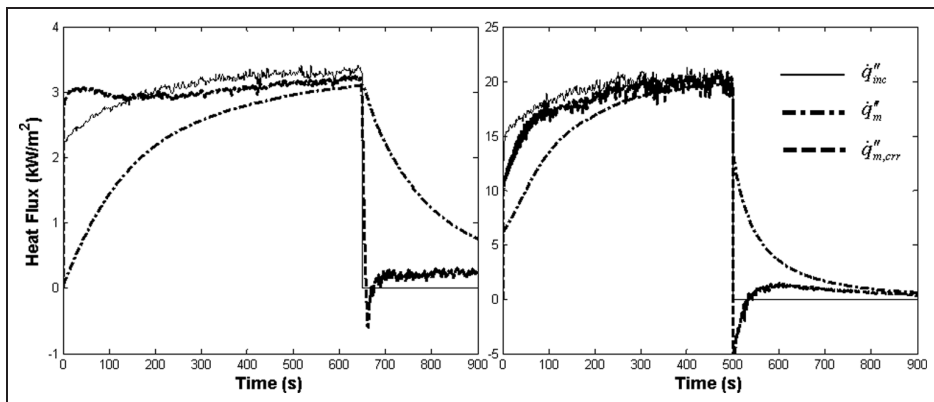


Figure 6. Examples of plate gage giving incident radiant heat flux.

equation (7) numerically. Clearly, the corrected flux is able to capture the transient behavior of the incident heat flux to a very high degree. It is essentially responding to a step change in the incident flux from zero to 3 and 20 kW/m^2 , respectively, and back to zero in both cases, as depicted in Figure 6. This represents a very extreme test of the plate gage's transient response and the first-order linear assumptions made previously for this device. There is an obvious undershoot in the corrected response when the incident flux is abruptly removed. This will not be an issue when the sensor is utilized within an actual enclosure fire as flame extinction never occurs in such a manner, and this is once again an extreme transient condition.

Compartment heat flux measurement methodology

Convective and radiative heat flux within the compartment were measured using a plate gage, thermopile gage, and thermocouple in an arrangement as depicted in Figure 7. This

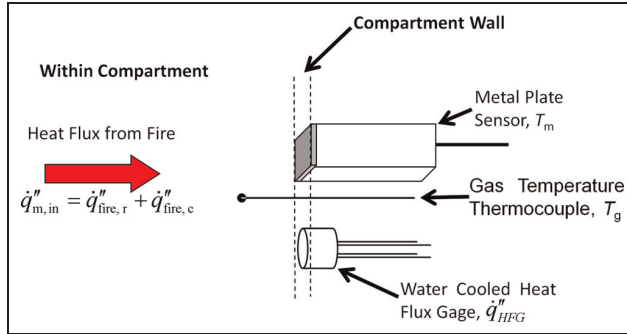


Figure 7. Schematic of arrangement of heat flux and temperature measurement devices.

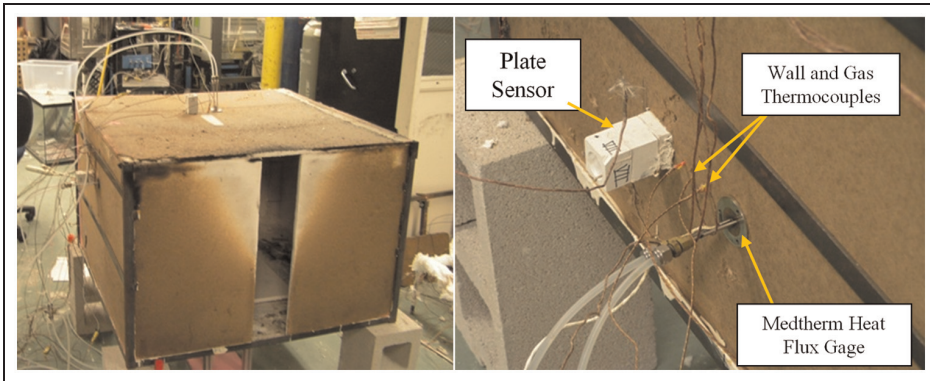


Figure 8. Actual arrangement of heat flux and temperature measurement devices.

setup was replicated at different locations within the actual compartment. Three locations were used: the ceiling, upper wall, and lower wall. The gas temperature thermocouple was a 0.13-mm K-type thermocouple. At each location at which the plate sensor and HFG were set up, an additional thermocouple was embedded in the wall to give a local wall temperature measurement. This was useful in determining the cool down or after extinction phase at which the local wall temperature exceeded the local gas temperature. The actual setup during experimental measurements can be seen in Figure 8.

The metal plate sensor–measured flux in a compartment fire as given by equation (8)

$$\left(\frac{mc}{A}\right)_m \frac{dT_m}{dt} + \dot{q}''_m + \epsilon_m \sigma T_m^4 = \dot{q}''_m + h_{fire,c} (T_g - T_m) \tag{8}$$

Analogous to equation (5), here h_{eff} is taken as

$$h_{eff,fire} = h_k + \sigma \epsilon_m (T_m^2 + T_\infty^2) (T_m + T_\infty) \tag{9}$$

There is no convective loss term, but now a convective addition is handled in the incident flux. Taking the plate heat flux (uncorrected) as

$$\dot{q}_m'' \equiv h_{eff,fire}(T_m - T_\infty) \quad (10)$$

Then, it follows from equations (8) and (9) that

$$t_{r,fire} \frac{d\dot{q}_m''}{dt} + \dot{q}_m'' = \dot{q}_{m,in}'' \quad \text{with } t_{r,fire} \equiv \frac{\left(\frac{mc}{A}\right)}{h_{fire,c}} \quad (11)$$

The incident heat flux to the plate sensor, $\dot{q}_{m,in}''$, is equal to the total incident radiation and convection heat flux from the compartment fire to the metal plate sensor (right-hand side of equation (8))

$$\dot{q}_{m,in}'' = h_{fire,c}(T_g - T_m) + \dot{q}_{fire,r}'' - \varepsilon_m \sigma T_\infty^4 \quad (12)$$

and correspondingly, the incident heat flux to the water-cooled HFG is

$$\dot{q}_{HFG}'' = h_{fire,c}(T_g - T_\infty) + \dot{q}_{fire,r}'' \quad (13)$$

The difference between the heat flux gage-measured flux, equation (13), and the metal plate sensor-measured flux, equation (12), gives the convective heat transfer coefficient as

$$h_{fire,c} = \frac{\dot{q}_{HFG}'' - \dot{q}_{m,in}'' - \varepsilon_m \sigma T_\infty^4}{(T_m - T_\infty)} \quad (14)$$

Results and discussion

Three locations were used in each compartment: ceiling, upper wall, and lower wall. Herein, there will be no discrimination between these locations as present results indicate that there are no substantive differences at each of these locations in these fully developed fires. Figure 9 is an indication of the gas temperature levels measured, and Figure 10 is illustrative

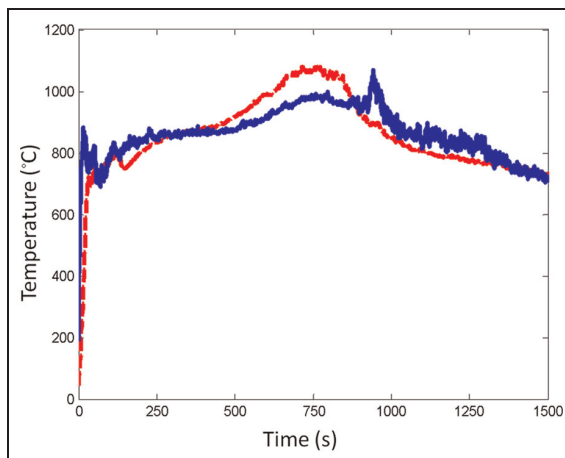


Figure 9. Illustration of compartment gas temperature for a repeated experimental condition.

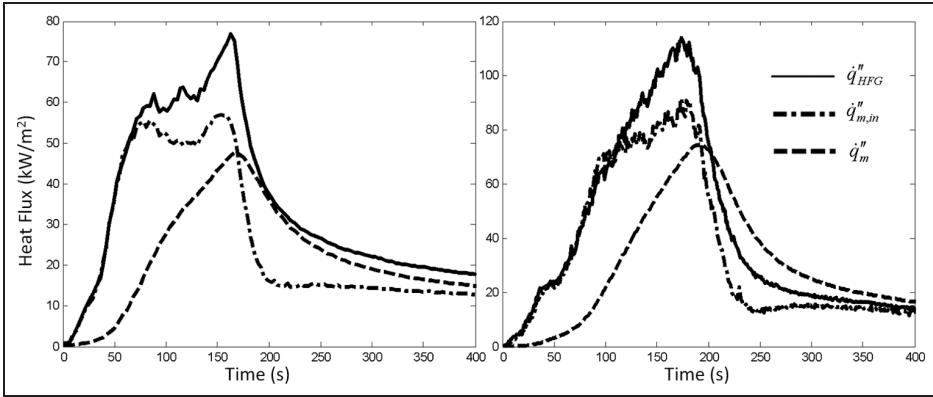


Figure 10. Illustration of compartment heat flux levels.

of the heat flux levels. Compartment gas temperature reached 1100°C and heat flux of 200 kW/m² was measured.

Convective heat transfer coefficient

An illustration of the computed convective heat transfer coefficient per equation (14) along with processing the parameters of equations (8) to (14) is shown in Figure 11. Its order of magnitude (say 50 W/m² K) and a maximum incident heat flux of 200 kW/m² at gas temperatures of 1000°C suggest a convective portion of the total of about 50 kW/m². Hence, in these fires, convection can be up to 25% of the total heat flux received by a flat surface in the compartment.

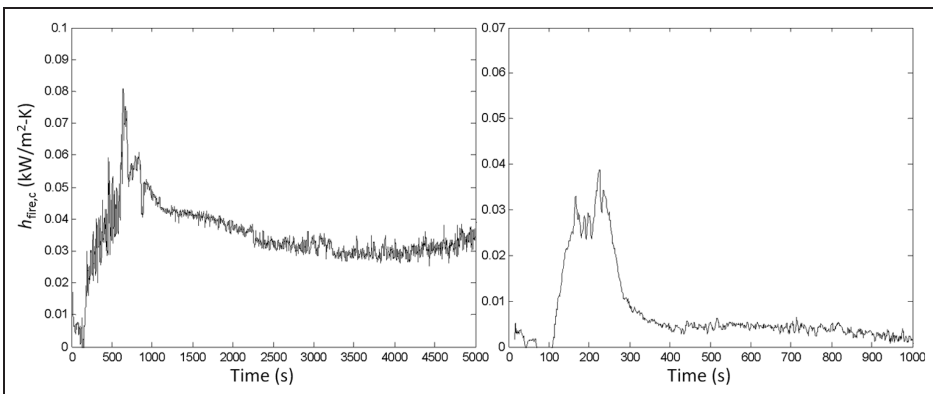


Figure 11. Illustration of determined convective heat transfer coefficient during a fire.

These convective heat transfer coefficient results were arranged according to their corresponding local gas temperatures recorded over time in a given run. Figure 12 gives some results for two of the measuring points in a compartment fire. While some differences exist

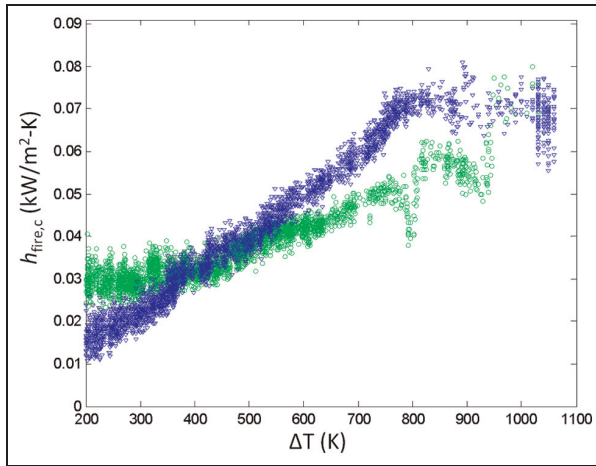


Figure 12. Illustration of the heat transfer coefficient at two measuring stations after extinction.

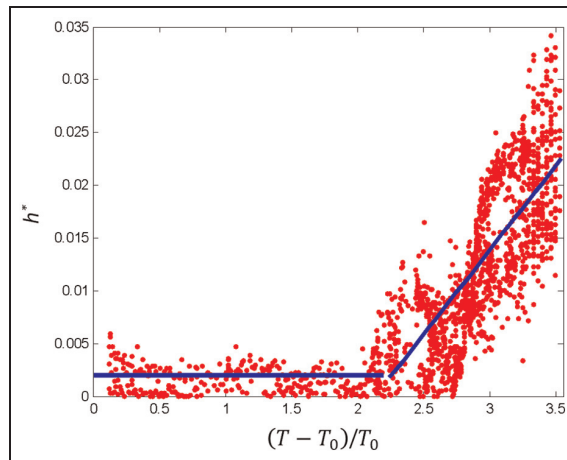


Figure 13. Dimensionless heat transfer coefficient during flaming.

for the locations, for these fully developed large fires, a definitive trend with location was not perceived. Then, all these results were presented, for both the wall and ceiling locations, in total in terms of the temperature increase over ambient temperature. This temperature difference is the driving force for flow into the compartment opening.

The heat transfer coefficient is seen to increase with temperature difference. As scale was varied in these experiments, the effect of scale was accounted for by considering a dimensionless heat transfer coefficient as the Stanton number expressed in terms of a characteristic velocity in natural convection. The height of the compartment was taken as the characteristic length scale, l . Figures 13 and 14 show the total results plotted for both the burning period and the cooling or extinction period that follows. Data from all three scales have been

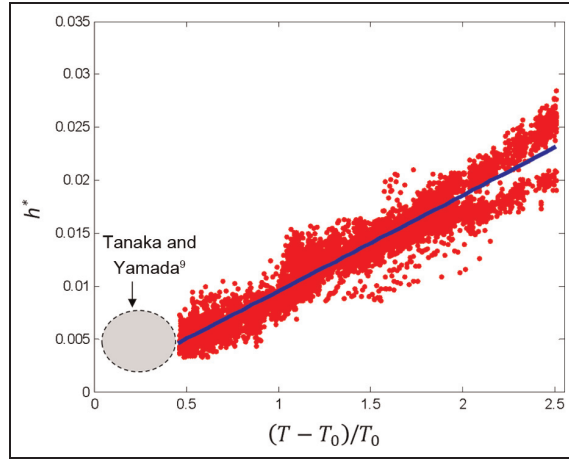


Figure 14. Dimensionless heat transfer coefficient for the cooling or extinction phase.

incorporated into Figures 13 and 14. It is seen that the data of Tanaka and Yamada⁹ for small fires comply with the correlation. Fits of these data indicate approximate formulas for the earlier extinction case as

$$h^* = \frac{h_{fire,c}}{\rho_{\infty} c_p (gl)^{1/2}} = \begin{cases} 2 \times 10^{-3} & \frac{\Delta T}{T_{\infty}} < 2 \\ 16 \times 10^{-3} \frac{\Delta T}{T_{\infty}} & \frac{\Delta T}{T_{\infty}} \geq 2 \end{cases} \quad (15)$$

and for after extinction as

$$h^* = \frac{h_{fire,c}}{\rho_{\infty} c_p (gl)^{1/2}} = 9.9 \times 10^{-3} \frac{\Delta T}{T_{\infty}} \quad (16)$$

Concluding remarks

Using a heated plate HFG and a water-cooled gage, the convective heat transfer coefficient was measured and correlated over a range of temperatures in flaming and cooling periods for compartment fires. Heat flux could attain levels between 100 and 200 kW/m² with convection accounting for up to 25%. The results could be applied to improve empirical estimates of the rate of cooling in compartment fires and its impact on structure integrity.

Funding

This study was performed at the University of Maryland and supported by the National Science Foundation under Award Number 0301643.

References

- 1. McGrattan K, McDermott R, Hostikka S, et al. *Fire dynamics simulator (version 5) user's guide*. NIST Special Publication, 1019-5, October 2010. Washington, DC: US Government Printing Office.

2. Veldman CC, Kubota T and Zukoski EE. *An experimental investigation of the heat transfer from a buoyant gas plume to a horizontal ceiling—part 1 unobstructed ceiling*. National Bureau of Standards, NBS-GCR-77-97, June 1975.
3. Zukoski EE and Kubota T. *An experimental investigation of the heat transfer from a buoyant gas plume to a horizontal ceiling—part 2 effects of ceiling layer*. National Bureau of Standards, NBS-GCR-77-98, September 1975.
4. You HZ and Faeth GM. Ceiling heat transfer during fire plume and fire impingement. *Fire Mater* 1979; 3: 140–147.
5. Cooper LY. Convective heat transfer to ceilings above enclosure fires. *Symposium (International) on Combustion* 1982; 19: 933–939.
6. Cooper LY and Stroup DW. Thermal response of unconfined ceilings above growing fires and the importance of convective heat transfer. *J Heat Transf* 1987; 109: 172–178.
7. Beyler CL. Fire plumes and ceiling jets. *Fire Safety J* 1986; 11: 53–75.
8. Alpert RL. Convective heat transfer in the impingement region of a buoyant plume. *J Heat Transf* 1987; 109: 120–124.
9. Tanaka T and Yamada S. Reduced scale experiments for convective heat transfer in the early stages of fire. *Int J Eng Perform Fire Codes* 1999; 1: 196–203.
10. Perricone J, Wang M and Quintiere JG. Scale modeling of the transient thermal response of insulated structural frames exposed to fire. *Fire Technol* 2008; 44: 113–136.
11. Wang M, Perricone J, Chang PC, et al. Scale modeling of compartment fires for structural fire testing. *J Fire Prot Eng* 2008; 18: 223–240.
12. Perricone J. *Scale modeling of the transient behavior of wood crib fires in enclosures*. Master's Thesis, University of Maryland, College Park, MD, 2005.
13. Wang M. *Scale modeling of structural behavior in fire*. PhD Thesis, University of Maryland, College Park, MD, 2006.
14. Veloo PS. *Scale modeling of the transient behavior of heat flux in enclosure fires*. Master's Thesis, University of Maryland, College Park, MD, 2006.
15. Wickström U. The plate thermometer—a simple instrument for reaching harmonized fire resistance tests. *Fire Technol* 1994; 30: 195–208.
16. Wickström U. The adiabatic surface temperature and the plate thermometer. *Fire Safety Sci* 2011; 10: 1001–1011.
17. Lennon PF and Silcock GWH. An investigation of the ability of a thin plate heat flux device to determine the incident heat fluxes during enclosure fires. *Int J Eng Perform Fire Codes* 2001; 3: 1–15.
18. Lennon PF and Silcock GWH. A preliminary investigation into the partitioning of the convective and radiative incident heat flux in real fires. *Fire Technol* 2006; 42: 109–129.
19. Zhang J and Delichatsios MA. Determination of the convective heat transfer coefficient in three-dimensional inverse heat conduction problems. *Fire Safety J* 2009; 44: 681–690.

Appendix I

Notation

c_p	specific heat
g	gravity
h^*	dimensionless heat transfer coefficient
$h_{e,plate}$	plate sensor heat transfer coefficient during calibration
h_{eff}	effective radiative, conductive, and convective heat transfer coefficient during calibration
$h_{eff,fire}$	effective combined radiative and conduction heat transfer coefficient during fire
$h_{fire,c}$	plate sensor convective heat transfer coefficient during fire
h_k	conductive heat transfer coefficient
l	characteristic length, compartment height
$(mc/A)_m$	heat capacity per unit area for plate sensor
$\dot{q}''_{cond,m}$	conduction losses from plate sensor
$\dot{q}''_{fire,r}$	radiative heat transfer from fire
\dot{q}''_{HFG}	incident heat flux to water-cooled HFG during fire
\dot{q}''_{inc}	incident heat flux during calibration
\dot{q}''_m	plate sensor actual measured heat flux

$\dot{q}_{m,corr}''$	time response corrected plate sensor heat flux
$\dot{q}_{m,in}''$	total incident radiative and convective heat transfer from fire to plate sensor
t	time
t_r	time response of plate sensor during calibration
$t_{r,fire}$	time response of plate sensor during fire
T_g	gas temperature in boundary layer near plate sensor
T_m	plate sensor temperature
T_∞	ambient temperature
α_m	absorptivity of plate sensor
ε_m	emissivity of plate sensor
ρ_∞	density
σ	Stephan–Boltzmann constant
ΔT	temperature difference between gases and wall surface in boundary layer near plate sensor

Author biographies

Peter S Veloo is a Postdoctoral Research Associate at the Department of Mechanical and Aerospace Engineering at Princeton University, Princeton, New Jersey, USA.

James G Quintiere is a Professor Emeritus at the Department of Fire Protection Engineering at the University of Maryland, College Park, Maryland, USA.